JOURNAL OF GEOPHYSICAL RESEARCH, VOL. 115, D02105, doi:10.1029/2009JD011858, 2010



# High Resolution Dynamics Limb Sounder measurements of gravity wave activity in the 2006 Arctic stratosphere

C. J. Wright,[1] S. M. Osprey,[1] J. J. Barnett,[1] L. J. Gray,[2] and J. C. Gille[3]

Received 5 February 2009; revised 22 September 2009; accepted 6 October 2009; published 23 January 2010.

[1] Observations from the High Resolution Dynamics Limb Sounder (HIRDLS) instrument on NASA's Aura satellite are used to quantify gravity wave momentum fluxes in the middle atmosphere. The period around the 2006 Arctic sudden stratospheric warming (SSW) is investigated, during which a substantial elevation of the stratopause occurred. Analysis of the HIRDLS results, together with analysis of European Centre for Medium-Range Weather Forecasting zonal winds, provide direct evidence of wind filtering of the gravity wave spectrum during this period. This confirms previous hypotheses from model studies and further contributes to our understanding of the effects of gravity wave driving on the winter polar stratopause.

**Citation:** Wright, C. J., S. M. Osprey, J. J. Barnett, L. J. Gray, and J. C. Gille (2010), High Resolution Dynamics Limb Sounder measurements of gravity wave activity in the 2006 Arctic stratosphere, *J. Geophys. Res.*, *115*, D02105, doi:10.1029/2009JD011858.

## 1. Introduction

[2] Recent studies [*Siskind et al.*, 2007; *Manney et al.*, 2008b] have described a significant vertical displacement of the 2006 Arctic stratopause, with temperatures at 0.01 hPa exceeding 250 K and unusually cold temperatures at the usual stratopause height. Observations from the Microwave Limb Sounder (MLS) instrument on the Aura satellite and the Sounding of the Atmosphere by Broadband Emission Radiometry (SABER) instrument on the TIMED satellite, among others, showed a steady drop in the polar stratopause height over the course of January 2006, followed by the breakdown of the polar vortex. After around two and a half weeks, a cool high-latitude stratopause reformed at high altitude, remaining separated from that at low and mid-latitudes for a further month.

[3] To more fully understand the processes taking place during this period, *Siskind et al.* [2007] simulated the middle atmospheric temperature structure at high latitudes for early 2005 and 2006 using the NOGAPS-ALPHA GCM, extended to reach a top model height of $10^{-4}$ hPa and with improved radiative forcing and ozone climatology. Two different models for mesopheric gravity wave drag (GWD) were used, one on the basis of simple Rayleigh friction and another using a subgrid-parameterized orographic gravity wave drag (OGWD) model that also accounted for wave-filtering; they were then compared against a control run with no GWD. Of these, only the OGWD model captured the key morphology of both years. Further, the OGWD runs suggested that the changed stratopause was related to strongly reduced levels of mesospheric GWD because of wave-filtering in the stratosphere by atypically weak lower stratospheric zonal winds.

[4] Recent measurements with the High Resolution Dynamics Limb Sounder (HIRDLS) instrument on NASA's Aura satellite allow us to measure atmospheric temperature profiles on a global scale with unprecedentedly high vertical resolution, allowing us to directly observe a significant proportion of the gravity wave spectrum of the middle atmosphere. Here, we analyze results obtained from HIRDLS data regarding gravity wave activity in the stratosphere during this period by comparison with other, more typical, years, and provide possible explanations for the results obtained using wind data from the European Centre for Medium-Range Weather Forecasting (ECMWF) operational analyses.

## 2. High Resolution Dynamics Limb Sounder

[5] The HIRDLS [*Gille et al.*, 2003, 2008] is a 21-channel limb-scanning infrared radiometer aboard the Aura satellite, designed to make global measurements of atmospheric radiances at a vertical resolution finer than that of previous instruments. Aura is a sun-synchronous satellite in a low polar orbit, completing an orbit once every 99 min.

[6] During launch, the instrument suffered a partial failure, with unexpectedly uniform and high radiances measured throughout the field of view and damping experienced while using the instrument scan mirror elevation mechanism of the instrument. Further tests [*Barnett et al.*, 2005] concluded that this was because of a blockage covering a significant portion of the viewing window, now believed to be a piece of Kapton insulating material that came loose during launch. Significant work [*Gille et al.*, 2008] has been undertaken to introduce corrections for the errors introduced by this blockage, and certain data products, including temperature and pressure, are now becoming available for scientific use.

[1] Atmospheric, Oceanic, and Planetary Physics, Department of Physics, University of Oxford, Oxford, UK.
[2] Department of Meteorology, University of Reading, Reading, UK.
[3] Center for Limb Atmospheric Sounding, University of Colorado at Boulder, Boulder, Colorado, USA.


0148-0227/10/2009JD011858$09.00

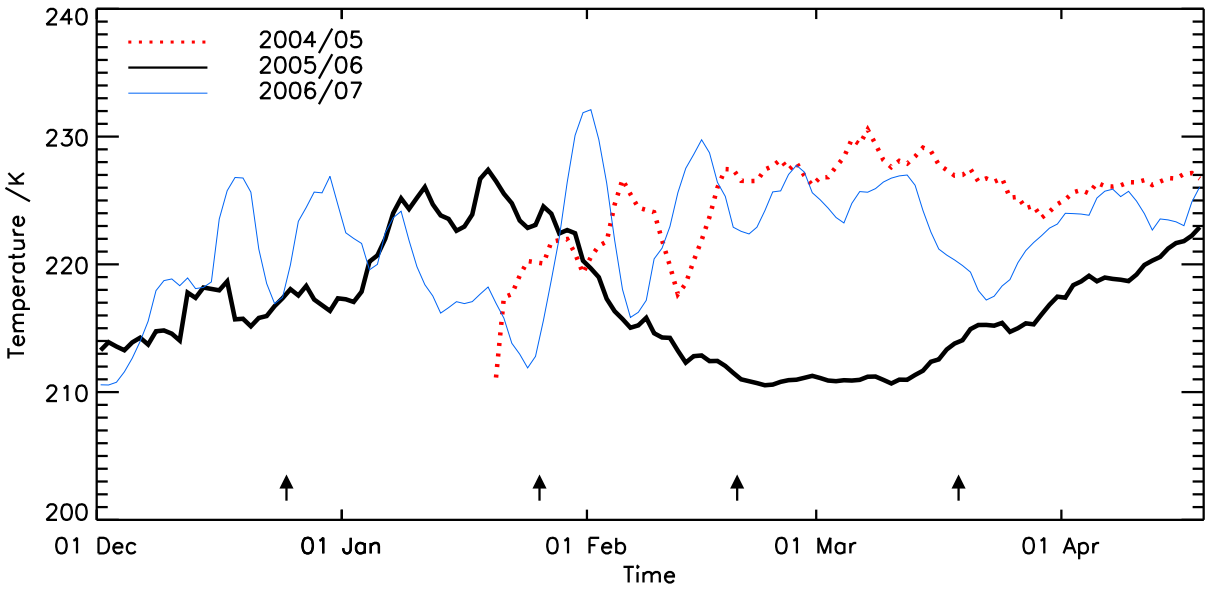


**Figure 1.** The 10 hPa winter time series of zonal mean temperatures at 60°N measured by HIRDLS for 2004/2005, 2005/2006, and 2006/2007. Note the substantially reduced temperatures during February and March 2006 relative to the other 2 years. Arrow marks in this and subsequent plots indicate the four days detailed in Figure 5 and discussed in more detail in the text.

[7] The original specification for the HIRDLS mission called for the instrument to scan at a range of azimuths, providing orbit-to-orbit coverage of about 400–500 km. However, due to the blockage, measurements can only be made at a single azimuth, lying at 47° to the orbital plane of the satellite on the side away from the sun. Because of this limitation, the profiles measured by the instrument in operation have a much closer horizontal spacing than originally planned, with a horizontal along-track spacing between profiles of about 75–100 km. This strongly facilitates gravity wave studies, by allowing the detection of much smaller scale horizontal structures than would have been made under the original mission profile. The vertical projection of the field of view at the limb is about 1 km, and with some oversampling, the potential exists for vertical resolution <1 km [*Alexander et al.*, 2008; *Gille et al.*, 2008; *High Resolution Dynamics Limb Sounder Team*, 2008].

[8] Profiles are most heavily concentrated around the northern and southern turnarounds at about 80°N and about 62°S due to the orbital path of the satellite and the way in which the blockage restricts the viewing angle. The orbital path of Aura remains the same throughout the year, in contrast to that of (for example) SABER, which uses a 60 day "yaw" cycle to alternate between coverage of high latitudes in alternate hemispheres. This allows HIRDLS to study the development of selected parts of the high-latitude atmosphere over extended periods.

[9] Following revisions to the scanning pattern used to minimize the effects of the blockage, HIRDLS began collecting data on the 21st of January 2005 [*High Resolution Dynamics Limb Sounder Team*, 2008], with some intermittency in the temporal data coverage for a few weeks after this. This study uses HIRDLS V004 data for the period 2005–2007: this is the most current version available. All data, both HIRDLS and ECMWF, have been smoothed by 5 days postprocessing: this is to allow comparison with the values obtained for momentum flux, which exhibit significant variation between days and hence require some smoothing to allow conclusions to be drawn.

## 3. Temperature and Wind Trends During Arctic Winter 2005/2006

[10] Figure 1 shows a time series of zonal mean temperature at 10 hPa, 60°N over the three consecutive Northern Hemisphere winters 2004/2005, 2005/2006, and 2006/2007, as measured by HIRDLS. Compared with the other 2 years shown, a clear difference can be observed in the data for 2005/2006. The temperature rises sharply in early-to-mid January 2006, followed by an equally sharp fall in late January, and does not recover to its typical levels until late March-early April.

[11] This behavior is consistent with that described by other studies [e.g., *Manney et al.*, 2008a, 2008b; *Hoffmann et al.*, 2007] as a manifestation of a major SSW (defined as having easterly winds down to 10 hPa at 60°N) during January 2006, with a strong reversal of 1 hPa zonal winds in mid-January followed around a week later by a reversal of the 10 hPa zonal winds above 60°N and a decline in mesospheric wave-one amplitude.

[12] *Hoffmann et al.* [2007] discuss MF radar and meteor radar observations of mesospheric (70–94 km) winds and temperatures during the same period. In their results, easterly winds descend through the mesosphere during January, followed by a period of intensified westerly winds at all heights in February. This occurred while stratospheric planetary wave-one amplitudes decreased during late January. Easterly winds then once again descend from the upper to lower mesosphere during March and April, and remain at all heights thereafter. Both periods of easterly winds are

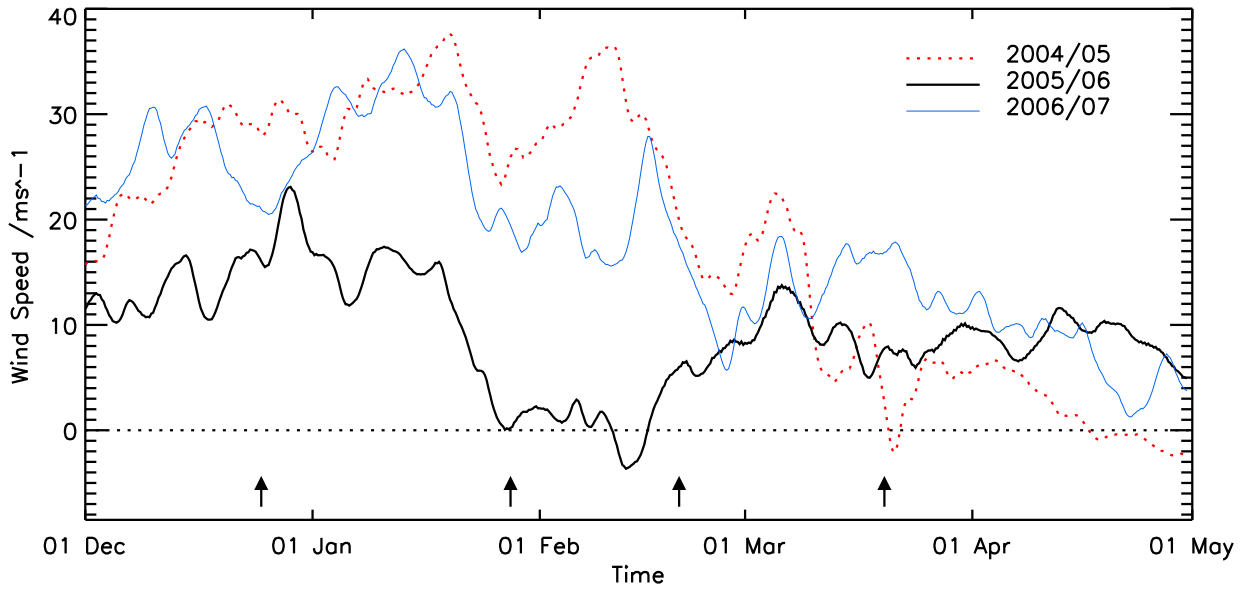


**Figure 2.** The 50 hPa winter time series of zonal mean zonal winds at 60°N measured by ECMWF. Note the prolonged period of substantial easterly (negative zonal) winds during late January to early February 2006 by comparison to the other 2 years.

followed by a prolonged period of reduced gravity wave activity throughout the mesosphere, especially marked in the upper stratosphere-lower mesosphere (55–70 km) region, where activity falls almost to zero. During the January period, the region of low activity is located almost entirely below 65 km, while the more prolonged period beginning in March and April exists at all levels below about 80 km.

[13] Figure 2 shows a time series of zonal mean winds at 50 hPa over the same period, obtained from the ECMWF operational analyses. While the ECMWF operational analyses over this period do not fully capture the raised stratopause due to lack of observations at high altitudes [*Manney et al.*, 2008b], at low and midstratospheric altitudes the wind speed data are well constrained by observations. Winds in 2004/2005 and 2006/2007 show a steady drop with time, consistent with the usual climatological trend. The year 2005/2006 once again appears substantially different: zonal winds are significantly reduced by comparison with 2004/2005 and 2006/2007 and there is a prolonged period during late January and early February of easterly and near-zero westerly zonal winds. This period of reduced westerlies begins in early January, slightly after the time at which the mesospheric winds observed by *Hoffmann et al.* [2007] reach the lowest extent of the mesosphere. This suggests continuity with the observed descent, and is likely associated with a change in the temperature gradient caused by the earlier SSW.

[14] *Manney et al.* [2008b] also discusses the amplitude of planetary wave-one features in the stratosphere and mesosphere. Figure 3 of *Manney et al.* [2008b], drawing from multiple sources, showed that the wave-one amplitude was high at all levels from about 50 hPa up to about 0.01 hPa throughout December 2005 and most of January 2006, suddenly collapsing at the same time the wind at these altitudes reversed, around the 20th of January. A lower intensity wave-one then formed at high altitudes (about 0.02 hPa), which descended in altitude slowly during February and March. Wave-two amplitudes followed a similar trend in December and January, collapsing around the 20th of January, but did not reform at high altitude with the original intensity.

## 4. Detection of Gravity Wave Momentum Flux Using HIRDLS

[15] The method used to calculate the along-track component of the vertical flux of horizontal momentum (hereafter referred to as "momentum flux") due to gravity waves in the HIRDLS data is that outlined by *Alexander et al.* [2008]. All available daily vertical temperature profiles in the height range 100–0.1 hPa are averaged into 2.5° latitude × 12° longitude bins. Planetary-scale oscillations (wavenumbers 1–3), together with an overall mean, are calculated for each height level. The wavenumber 1–3 component and the underlying mean are then removed from the individual profiles according to which bin the profiles fall into. From this, we obtain profiles of temperature perturbation due to nonplanetary waves.

[16] The S-transform [*Stockwell et al.*, 1996] is then applied to the perturbation profiles. This returns, for each profile, the variation of the spectral properties of the signal $\tilde{T}(z, \lambda_z)$ with respect to spatial distance, that is to say the wavelengths $\lambda_z$ present at each height level $z$, as a complex-valued function of height. For each adjacent profile pair $(i, i+1)$ the cospectrum

$$C_{i,i+1} = \tilde{T}_i \tilde{T}^*_{i+1} \tag{1}$$

and covariance spectrum $|C_{i,i+1}|$ are then computed, and the maximum in the covariance spectrum located for wavelengths less than 16 km, giving the dominant vertical

wavelength present at each height $\lambda_z(z)$. We also compute the covarying amplitude

$$\hat{T}_{i,i+1} = \sqrt{|C_{i,i+1}|} \tag{2}$$

and phase difference between profiles

$$\Delta\phi_{i,i+1} = \arctan\left(\frac{\mathrm{Im}(C_{i,i+1})}{\mathrm{Re}(C_{i,i+1})}\right). \tag{3}$$

[17] From the horizontal phase difference $\Delta\phi_{i,i+1}$ and distance between profiles $\Delta r_{i,i+1}$, we can then estimate the component of the horizontal wavenumber along the line joining the two profiles as

$$k_h = \frac{\Delta\phi_{i,i+1}}{\Delta r_{i,i+1}}, \tag{4}$$

and hence the magnitude of the component of the horizontal momentum flux $M_{i,i+1}$ along the line joining the two profiles as

$$M_{i,i+1} = \frac{\rho}{2}\lambda_z \frac{k_h}{2\pi}\left(\frac{g}{N}\right)^2\left(\frac{\hat{T}_{i,i+1}}{\overline{T}}\right)^2, \tag{5}$$

where $\rho$ is the background atmospheric density, $g$ the acceleration due to the Earth's gravity, N the Brunt-Väisälä frequency, and $\overline{T}$ the unperturbed background temperature [*Ern et al.*, 2004].

[18] The derivation of equation (5) [*Ern et al.*, 2004] assumes that the gravity waves being analyzed can be considered to be in the midfrequency range, such that $N \gg \hat{\omega} \gg f$, where $f$ is the Coriolis parameter $f = 2\Omega\sin(\Phi)$, $\Omega$ is the Earth's rotation frequency, $\Phi$ is the latitude of the wave, and $\hat{\omega}$ is the intrinsic wave frequency. This allows us to neglect the Coriolis effects because of the rotation of the Earth on the waves being studied. This can be justified by considering the full form of the gravity wave dispersion relation [*Fritts and Alexander*, 2003]

$$\hat{\omega}^2 = \frac{N^2(k^2+l^2) + f^2\left(m^2 + \frac{1}{4H^2}\right)}{k^2 + l^2 + m^2 + \frac{1}{4H^2}}, \tag{6}$$

where $k$ and $l$ represent the horizontal wavenumber of the wave, $k \sim l \sim 2\pi/\lambda_h$, $m$ represents the vertical wavenumber of the wave, $m \sim 2\pi/\lambda_z$, and $H$ represents the atmospheric scale height. For sampled horizontal wavelengths about 100 s of km, vertical wavelengths about 10 km, and typical stratospheric values for scale height (about 7 km) and the Brunt-Väisälä frequency (about 0.02 rad $s^{-1}$) in the stratosphere, it can be shown that the intrinsic wave frequency $\hat{\omega}$ is typical about $10^{-3}$ rad $s^{-1}$, falling comfortably between $N$ (about $10^{-2}$ rad $s^{-1}$) and $f$ (about $10^{-4}$ rad $s^{-1}$ at 60°N), and hence satisfying the midfrequency approximation.

[19] It should be noted that, because of the low probability of the horizontal wavevector of the gravity wave lying along the direction of travel of the instrument, horizontal wavenumbers are likely to be significantly undersampled. Therefore, $k_h$ and hence $M_{i,i+1}$ are likely to be underestimates [see e.g., *Ern et al.*, 2004], as they represent only the component of the wave lying in the direction of the HIRDLS scan track.

[20] Because of the instantaneous sampling of the waves and lack of two-dimensional data, the results obtained for momentum flux lack directional information [*Ern et al.*, 2006; *Alexander et al.*, 2008]; that is to say that the results represent a magnitude rather than a vector quantity. Waves with a horizontal wavelength along the scan track of shorter than the Nyquist sampling limit, less than about 150–200 km, do not contribute directly to the measured momentum flux because of the profile spacing. However, such waves can be aliased, leading to them being present in the detected signal with the wrong wavelength. The measurements may be sensitive to, but undersample, waves with horizontal wavelengths as short as about 10 km, and, consequently, they may contribute to the measured signal but with an underestimated momentum flux [*Alexander et al.*, 2008]. This is not a problem in the vertical direction, as the retrieval process suppresses features with vertical wavelengths less than the vertical sampling distance, about 1 km.

[21] Wavenumber 3 was used as the cutoff for mean removal for consistency with *Alexander et al.* [2008]. Previous studies, such as those of *Ern et al.* [2004], instead use a wavenumber 6 cutoff. To investigate the effect of this, monthly zonal means of observed momentum flux at all height levels for the northern hemisphere (cf., section 5) were investigated using a wavenumber 6 filter. No significant difference in the form of results was observed, although there was a slight increase in the measured values of $M_{i,i+1}$ by about 10% at all levels.

[22] Although it is difficult to validate the momentum flux measurements in such a way as to show that 2005 and 2007 are typical years in terms of momentum flux values, we can do so for temperature: the temperatures measured in 2005 and 2007 fall within one standard deviation of the long-term monthly mean temperatures (223.5 ± 3.4 K for February, 223.9 ± 3.7 K for March, derived from ECMWF ERA-40 data for the period 1979–1999), while those for late February and March 2006 fall substantially outside this range.

## 5. Measurements of Momentum Flux in the 2005/2006 Arctic Stratosphere

[23] Figure 3 shows the zonal average of the momentum flux at 10 hPa, 60°N. The data available for 2 years during the period from late January until early February show a peak. There is then a steady falloff observed in all 3 years during February and March to a low-level, at which it stays throughout the summer before rising again in late November (not shown). A sharp reduction over the period of interest is seen in 2006 when compared to the data of other 2 years. A steady drop off in momentum flux levels is observed from mid-January onward, recovering slightly toward the end of February before merging back into the general seasonal trend by late March. The scale of this decline is significant as a proportion of the mean value in the other years, with measured levels in mid-late February of 0.2 mPa substantially lower than the average for 2005 and 2007 during this period of around 0.6 mPa, and represents a drop in measured momentum flux by two-

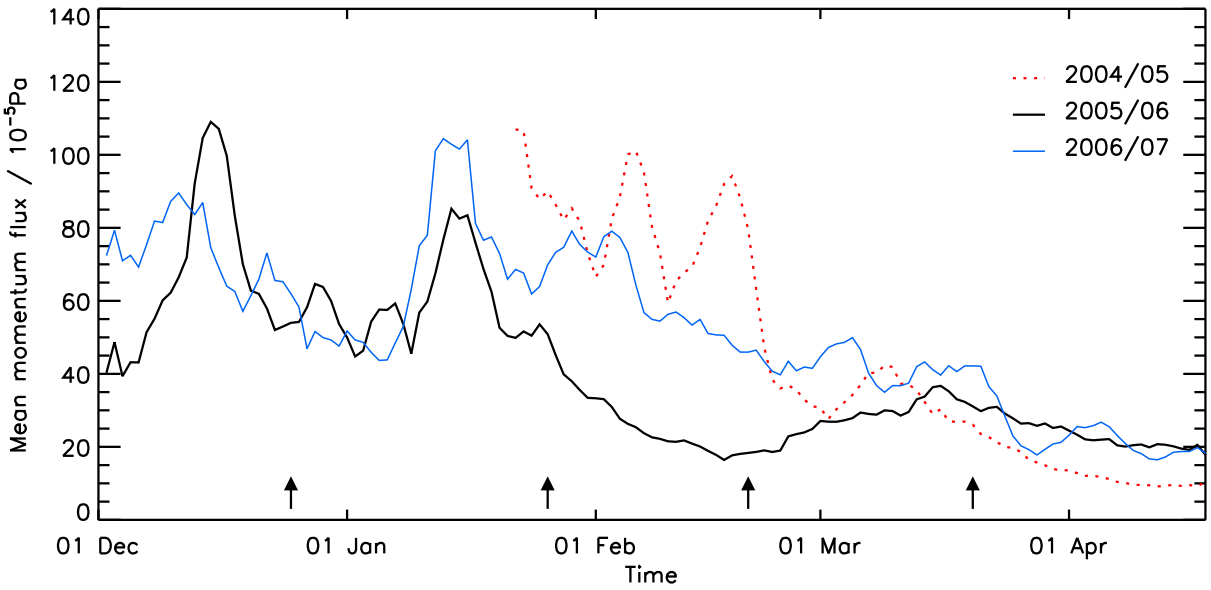


**Figure 3.** The 10h Pa winter time series of zonal mean momentum at 60°N measured by HIRDLS for 2005, 2006, and 2007. Note the reduced level between late January and early March 2006 compared to the other 2 years.

thirds. We can compare these results for momentum flux to the stratopause height results of [*Manney et al.*, 2008b]. Figure 4 of [*Manney et al.*, 2008b] shows a steady descent of the stratopause (calculated as the "warm point" of the middle atmosphere) at 60°N, beginning in the second week of January and dropping steadily until the last week of January. A new stratopause then reforms at about 70 km and begins to descend slowly, stabilizing at about 50 km in mid-March. This suggests a strong link between the stratopause height and the reduction observed in the measured momentum flux.

[24] Figures 4d–4f shows daily-mean HIRDLS-derived zonally averaged gravity wave momentum flux in the Northern Hemisphere for the 20th of February of the three consecutive years 2005–2007, as a function of latitude and height. Monthly mean calculations show broadly similar results, and preliminary processing of a fourth winter (2007/2008) of data, which are still undergoing validation, also serve to confirm that 2006 is anomalous, with broadly similar temperatures and momentum fluxes observed in 2008 to those in 2005 and 2007. As discussed in section 4, Figure 4 represent lower bounds to the actual momentum flux present in the atmosphere.

[25] In February 2005 and 2007 (Figure 4, left and right, respectively), a characteristic pattern is seen of medium-intensity momentum flux at equatorial latitudes, decreasing slightly in the region about 20°N–40°N before rising at latitudes poleward of 40°N. The intensity of the momentum flux drops off steadily but quickly with increasing height, consistent with density-dependent saturation processes in the upper stratosphere: at 100 hPa, values range from about 1.5 mPa at equatorial latitudes to a strong peak of >3 mPa at high latitudes (60°N–80°N), while at 10 hPa values ranging from about 0.3 mPa at the equator to 0.6 mPa at 70°N.

[26] The distribution for 2006 (center), however, clearly shows a marked reduction of measured momentum fluxes at all heights for latitudes north of 40°N. Momentum flux levels also fall with increasing latitude. At the 100 hPa level, values range from about 1.5 mPa at the equator through a minor peak of about 3.0 mPa around 35°N–40°N before falling away steadily to a low of 2.5 mPa at 60°N, and at the 10 hPa level values rise from around 0.2 mPa at the equator to a high level of about 0.3 mPa at 40°N before falling away rapidly to less than 0.15 mPa at 80°N. These values are consistent with the conclusions of *Siskind et al.* [2007] that the level of gravity wave activity, and hence momentum flux because of gravity waves, was low in the Arctic stratosphere during this period, and requires further investigation. The small increase in values at 35°N–40°N probably represents the edge of the normal region of heightened momentum flux, with regions poleward of this reduced in magnitude.

## 6. Zonal Mean Temperature, Windspeed, and Momentum Flux as a Function of Latitude

[27] Figure 4 also shows Northern Hemispheric zonal mean temperature (Figures 4a–4c, from HIRDLS) and zonal mean zonal windspeed (Figures 4g–4i, from ECMWF operational analyses), for the 20th of February from 2005 to 2007. This day was selected as it lies in the trough of averaged momentum flux at 60°N in 2006 (Figure 3). Several differences can clearly be seen between 2006 (Figures 4b, 4e, and 4h) and the other 2 years. If we first consider zonal mean temperatures (Figures 4a–4c), a substantial difference can be observed poleward of 50°N, with temperatures at all heights substantially lower than usual. This is consistent with the raised stratopause described in *Siskind et al.* [2007]. There is also, as discussed previously, a strong difference in the recorded momentum flux values (Figures 4d–4f), and high-latitude momentum flux values are substantially lower in 2006 at all height levels. Figures 4g–4i, ECMWF zonal mean zonal wind speeds, show a different polar vortex strength at upper levels but

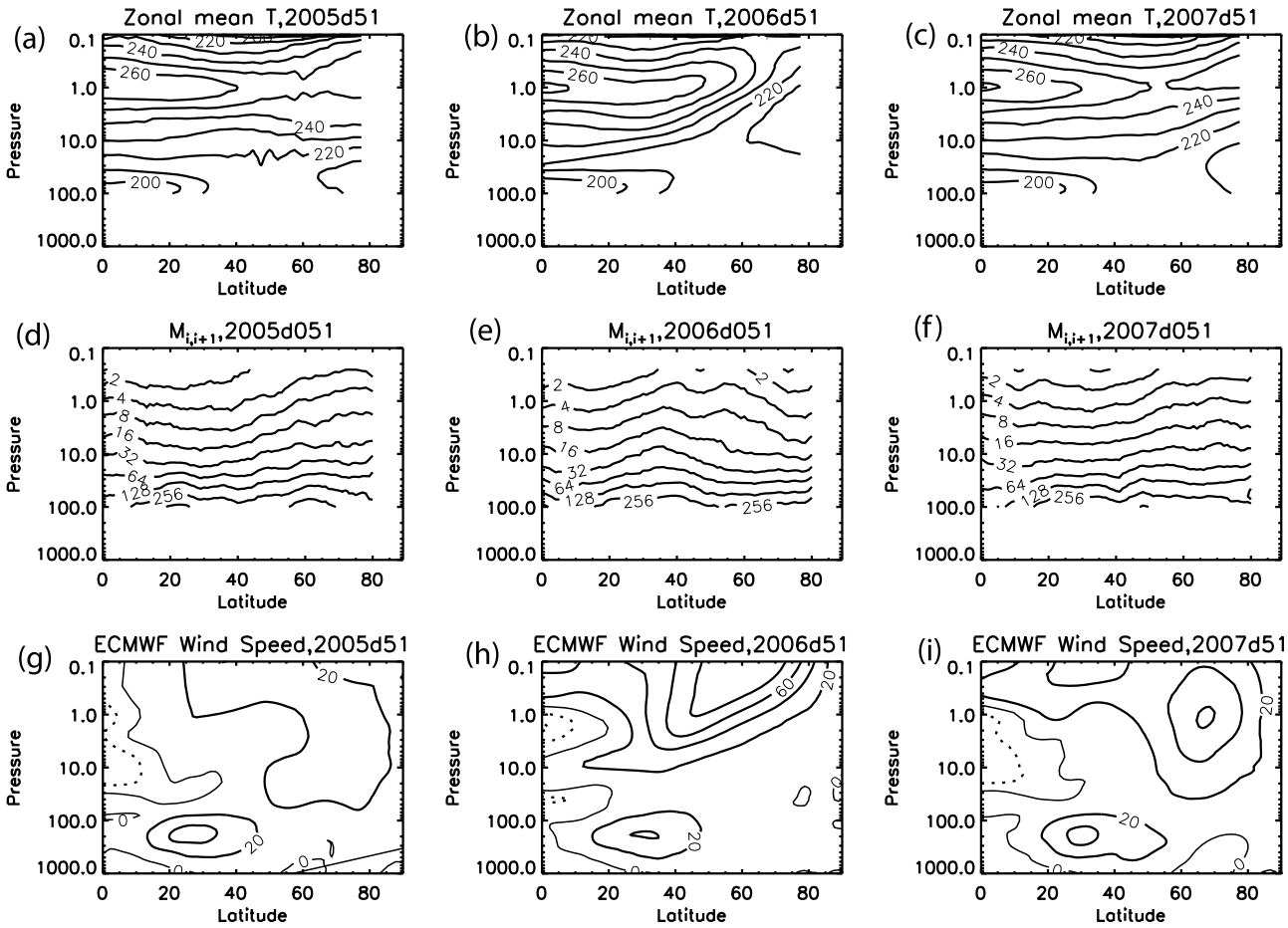


**Figure 4.** (a–c) Zonal mean temperature (in Kelvin), (d–f) zonal mean momentum flux (in $10^{-5}$ Pa), and (g–i) zonal mean zonal wind speed (in $ms^{-1}$) for the Northern Hemisphere on February 20th of 2005, 2006, and 2007. Note that, the number of levels in the ECMWF operational analysis model changed at the end of January 2006, giving finer resolution in the vertical after this date.

no dramatic difference between the 3 years below about 10 hPa.

[28] Figure 5 shows the same three parameters for four days during late 2005 and early 2006 to illustrate the development of the SSW and subsequent drop in momentum fluxes: the 25th of December (before the divergence of momentum flux from the usual seasonal trend), the 26th of January (the beginning of the trough of zonal mean zonal windspeed at 60N, 50 hPa (Figure 2)), the 20th of February (as before) and the 20th of March (after levels had merged back into the normal seasonal trend). These days are indicated by small black arrows on each of the relevant time series.

[29] Figures 5a, 5e, and 5i, showing results for the 25th of December 2005, show a zonal mean temperature profile with a typical separated stratopause. One distinct region stretches from the equator to midlatitudes, associated with adiabatic heating due to solar insolation. The second distinct stratopause, at high latitudes, is because of the gravity wave induced circulation [*Dunkerton*, 1978; *Murgatroyd and Singleton*, 1961].

[30] The momentum flux profile is of the form usually observed in the HIRDLS data for Northern Hemisphere winter, with a substantial peak recorded in measured momentum fluxes at high latitudes. The zonal wind distribution on the 25th of December is also typical for this time of year, consisting of a strong westerly zonal wind at high altitudes and latitudes and a smaller peak of easterly zonal winds near the equator.

[31] Distributions for the 26th of January (Figures 5b, 5f, and 5j) show a substantially different picture. The most obvious change is in $\overline{u}$ at high altitude, with a significant peak of easterly winds recorded poleward of 50°N indicative of the SSW. Momentum flux values have also changed significantly, with a marked decline from typical values everywhere poleward of around 50°N, leaving values at 60°N only very slightly above those at the equator and midlatitudes in contrast to their usual comparatively high values. Temperatures, meanwhile, show the early stages of the breakdown in the high-latitude stratopause described in *Siskind et al.* [2007] and *Manney et al.* [2008b]: this manifests itself as a temperature peak developing at about 10 hPa, representing a significant drop in the stratopause height. This is consistent with a substantial increase in the strength of the Brewer-Dobson circulation during the warming.

[32] By the 20th of February (Figures 5c, 5g, and 5k), the breakdown in the high Arctic stratopause has advanced

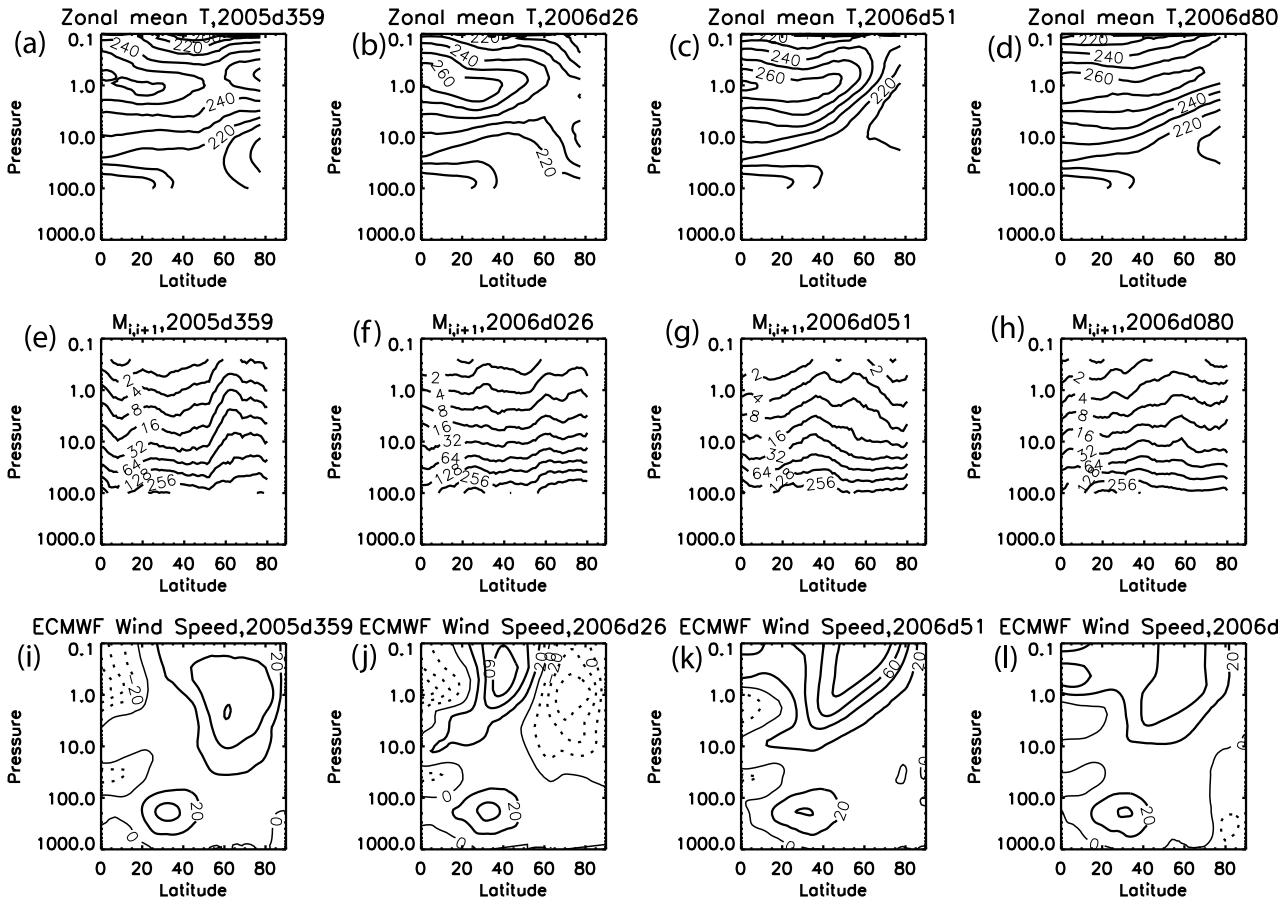


**Figure 5.** (a–d) Zonal mean temperature (in Kelvin), (e–h) zonal mean momentum flux (in $10^{-5}$ Pa), and (i–l) zonal mean zonal wind speed (in $ms^{-1}$) for the Northern Hemisphere on 4 days chosen over late 2005 and early 2006 (25th December 2005, 26th January 2006, 20th February 2006, and 20th March 2006, respectively). Note that, the number of levels in the ECMWF operational analysis model changed at the end of January 2006, giving finer resolution in the vertical after this date.

significantly, and the low-altitude stratopause of late January has disappeared. A new higher stratopause has formed at very high altitudes, with significantly lower temperatures than usual throughout the rest of the Arctic stratosphere. Momentum fluxes are further reduced, with high-latitude values less than those at the equator and in midlatitudes. By this point, however, high-altitude polar zonal mean zonal winds have become strongly positive again, heralding the beginning of the return of the Arctic atmosphere to a more normal state. By the 20th of March (Figures 5d, 5h, and 5l), all three parameters are back to their typical values and distributions for the time of year (taking into consideration that momentum flux values by this point of the winter are usually substantially lower at high latitudes than they would be in mid-late February), and the stratopause has returned to a more typical height.

## 7. Filtering by the Wind

[33] As shown by Figures 2 and 3, the period of rapid decline in momentum flux during late January and early February 2006 coincided with a period of easterly and strongly reduced westerly zonal mean winds, as described in section 3. This suggests a possible factor in the reduction in momentum flux levels.

[34] Gravity waves arise, mainly in the troposphere, from a range of sources, including orography, convection and wind shear. These waves exhibit a broad range of phase speeds [*Smith*, 1996]. The winds through which they travel, however, affect waves differently, depending upon the propagation direction [*Fritts and Alexander*, 2003]. Effects include Doppler-shifting, observational filter effects and critical-level wave filtering.

[35] Doppler-shifting represents the effect of (vertical) wind shear on vertically propagating waves [*Ern et al.*, 2004]. For example, positive (westerly) wind shear will Doppler-shift easterly traveling waves to lower vertical wavenumbers $m$. Conversely, negative (vertical) wind shear will move easterly waves to higher $m$ and toward critical levels. Second, the wind can Doppler-shift the waves out of the spectral region observable by HIRDLS. Since gravity waves are inherently broadband phenomena, this can give rise to apparent geographic, seasonal and vertical variations in observed gravity wave effects, without such variations existing [*Preusse et al.*, 2006; *Alexander*, 1998]. Finally, critical-level filtering represents the obliteration of waves as

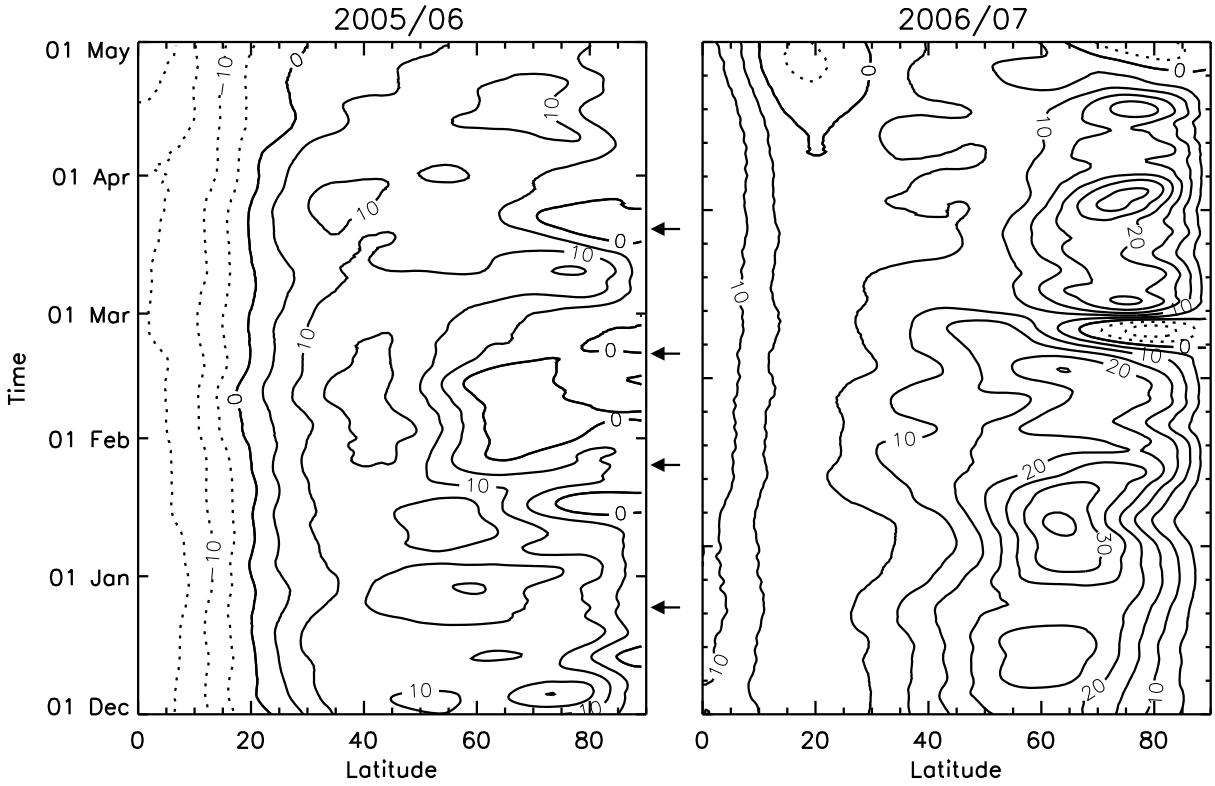


**Figure 6.** Latitude-time series of Northern Hemispheric ECMWF zonal winds at 50 hPa during (left) Arctic winter 2005/2006 and (right) Arctic winter 2006/2007. Negative windspeed contours are dashed.

the wave phase speed approaches that of the background flow.

[36] High-latitude tropospheric winds during winter are predominantly either low or slightly westerly (see, for example, Figures 4g–4i and 5i–5l), and hence any filtering of the gravity wave directional spectrum which takes place in the troposphere acts to reduce the proportion of westerly propagating waves. This means that any filtering that takes place leads to an imbalance in the directional spectrum of waves propagating vertically up into the stratosphere in favor of easterly propagating (westward) waves. In a typical Arctic winter, such as those for 2004/2005 and 2006/2007 shown in Figures 2 and 4, respectively, the prevailing wind direction in the lower stratosphere is also westerly. Since this is the same as the direction in which the tropospheric winds act, no significant additional filtering takes place in the lower stratosphere, leading to the relatively high momentum flux values.

[37] In 2006, however, a significant region of easterly wind exists from the 100 hPa level and upward during late January and early February, which functions to filter out gravity waves with easterly propagation directions above and beyond the usual westerly filtering taking place below. Since gravity waves propagating in both directions are now being filtered out, this leads to a significant reduction in the overall amount of momentum flux reaching middle and upper stratospheric heights, precisely what we observe in our momentum flux results.

[38] Figure 6 shows latitude-time series at 50 hPa for $\overline{u}$, obtained from ECMWF operational analyses. Data of 2006/2007 show a fairly typical Arctic winter. Winds poleward of 60°N are strong and zonal throughout the winter, slowly decreasing in strength and geographical extent as spring and summer approach. Markedly different behavior is seen in 2005/2006. In December and early January, zonal winds throughout the northern hemisphere are significantly weaker than in 2007, and wind speeds remain below 20 $ms^{-1}$ throughout the entire period shown. Negative zonal winds start to intrude from the pole in late January, reaching as far southwards as 60°N by early February, consistent with Figure 2. This also coincides with the beginning of the minimum of measured momentum fluxes at 10 hPa (Figure 3), suggesting a relationship between the low and negative zonal winds and the reduced momentum fluxes recorded.

[39] This is further corroborated by Figure 7, which shows zonal mean momentum fluxes at 60°N as a function of height and time over Arctic winter 2005/2006, with zonal mean zonal winds overplotted. As seen in Figure 6, wind speeds fall sharply toward the end of January and do not recover until early March, remaining weak, especially in the lower stratosphere. During this time, levels of momentum flux decrease markedly and remain low in the low-mid stratosphere. This further supports our hypothesis that anomalous easteries are associated with the reduced momentum flux observed by HIRDLS during this time.

[40] By late February, these easterly winds begin to disappear, although they continue to some degree until late March. Momentum flux values start to return toward more typical values, plateauing after a brief rise to join by late March into the general seasonal trend.

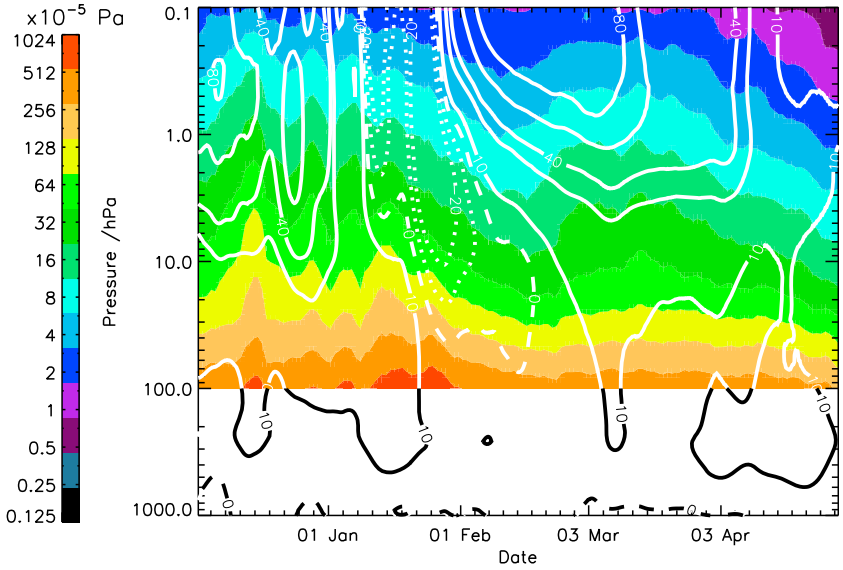


**Figure 7.** Height-time series of zonal mean momentum flux at 60°N during Arctic winter 2005/2006, with ECMWF zonal mean zonal winds overlaid. Wind contours are marked at −20, −10, 0, 10, 20, 40, 60, and 80 ms$^{-1}$. Negative contours are marked as dots, the zero contour as dashes, and positive contours as solid lines.

[41] As discussed in section 5, there is an increase in momentum flux values at 30°N–45°N in Figure 4e (February 2006). If this plot is compared with the latitude-time plot of zonal winds shown in Figure 6 (left), it can be observed that this region is outside the region of strongly reduced zonal winds during February 2006 at 50 hPa. This "bump" in the measured momentum flux field is probably the edge of the normal high momentum flux region, and hence supports our hypothesis of filtering by negative zonal winds in that the region outside the affected area is more normal.

[42] Finally, Figure 8 shows monthly mean polar stereographic plots of momentum flux for February 2005, 2006, and 2007, with zonal wind speeds overlaid. This illustrates several significant points. First, reduced momentum flux levels are observed in all locations with a strong signal in 2005 and 2007 throughout the entire Arctic region: that is to say, levels in 2006 are now low throughout the annular region surrounding the Pole. This contrasts with 2005 and 2007, where momentum fluxes are both generally higher and geographically more localized. For example, a maximum in momentum flux occurs around the southern tip of Greenland in 2005, a known region for orographic gravity waves [see e.g., *Leutbacher and Volkert*, 2000], but this region exhibits the same low values as all other longitudes in 2006. Second, the region of reduced momentum flux in 2006 overlaps significantly with the region of easterly and reduced westerly winds. Mean zonal winds for the month are below 10 ms$^{-1}$ throughout the Arctic, with regions of easterly wind overlying Siberia, Greenland and Northern Canada, whilst the main regions of low measured momentum flux lie at similar latitudes over all longitudes.

[43] It should be noted that reduced planetary wave activity may also have influenced the polar stratopause during these times: planetary wave amplitudes in the stratosphere were also significantly lower than normal during this

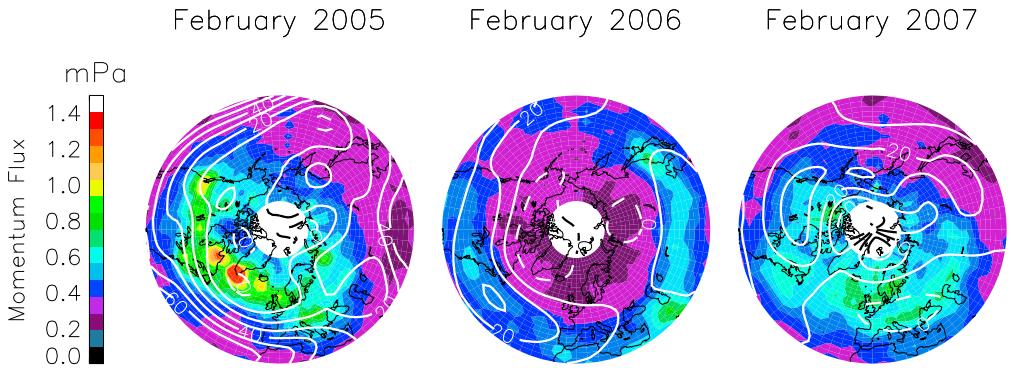


**Figure 8.** Polar stereographic monthly means of momentum flux at 10 hPa for February 2005, 2006 and 2007, with ECMWF-derived zonal winds at 50 hPa overplotted. Note the extended region of negative zonal winds at high latitudes in 2006, in contrast to 2005 and 2007.

period [*Manney et al.*, 2008b]. We provide evidence to support the idea that reduced gravity wave activity may also have played a role.

## 8. Conclusions

[44] HIRDLS data provide us with an opportunity to directly observe small vertical-scale gravity wave activity on a global scale, allowing us to make detailed estimates of momentum flux activity because of gravity waves throughout the middle atmosphere. This allows us to investigate the underlying gravity wave processes taking place during and after the anomalous change in stratopause height observed around the time of the Sudden Stratospheric Warming of January 2006. We examine the hypothesis of [*Siskind et al.*, 2007] that the behavior observed during this period was because of anomalously low gravity wave activity. Our observations suggest that the gravity wave momentum flux was significantly reduced during this period at latitudes above 50°N, starting in mid-January, and remained low throughout the remainder of January and February before resuming the general seasonal trend in mid-to-late March. Furthermore, this trend coincided with the stratopause height variations observed by *Manney et al.* [2008b].

[45] Analysis of our observations in combination with ECMWF operational analyses of zonal wind speed provide evidence of significant filtering by the background wind of the gravity wave spectrum during this period, contributing to the reduced gravity wave activity observed. We suggest that anomalous easterly and weak westerly winds in the lower stratosphere filter the gravity wave spectrum, reduced the intensity of easterly-propagating gravity waves which reach the middle stratosphere, and hence led to a significant reduction in the overall gravity wave spectrum reaching the middle atmosphere.

[46] Gravity wave driving is believed to exert significant control on mesospheric flow [*Holton*, 1983]. Because of the dynamical nature of the polar winter stratopause [*Hitchman et al.*, 1989], any change in gravity wave activity, such as that observed in Arctic winter 2006, can exert a significant effect on the temperature structure of the atmosphere in this region. As described in *Siskind et al.* [2007], this further helps to confirm our understanding that the polar winter stratopause is sensitive to gravity wave driving.

[47] **Acknowledgments.** ECMWF data used were obtained from the British Atmospheric Data Centre, http://badc.nerc.ac.uk. The work described in this paper was funded by the Natural Environment Research Council (NERC), UK. The work of JCG is funded by NASA's Aura satellite program under contract NAS5–97046. The authors would also like to thank M. J. Alexander for help with understanding the underlying physics and the S-transform gravity wave detection process, David Andrews for several useful comments on the manuscript, and the whole HIRDLS team for many years of dedicated work.

## References

Alexander, M. J. (1998), Interpretations of observed climatological patterns in stratospheric gravity wave variance, *J. Geophys. Res.*, *103*, 8627–8640.

Alexander, M. J., et al. (2008), Global estimates of gravity wave momentum flux from High Resolution Dynamics Limb Sounder (HIRDLS) observations, *J. Geophys. Res.*, D15S18, doi:10.1029/2007JD008807.

Barnett, J. J., C. L. Hepplewhite, L. Rokke, and J. C. Gille (2005), Mapping the optical obscuration in the NASA Aura HIRDLS instrument, *Proc. SPIE Int. Soc. Opt. Eng.*, *5883*, I1–I10.

Dunkerton, T. (1978), On the mean meriodional mass motions of the stratosphere and mesosphere, *J. Atmos. Sci.*, *35*(12), 2325–2333.

Ern, M., P. Preusse, M. J. Alexander, and C. D. Warne (2004), Absolute values of gravity wave momentum flux derived from satellite data, *J. Geophys. Res.*, *109*, D20103, doi:10.1029/2004JD004752.

Ern, M., P. Preusse, and C. D. Warner (2006), Some experimental constrains for spectral parameters used in the Warner and McIntyre gravity wave parameterization scheme, *Atmos. Chem. Phys.*, *6*, 4361–4381.

Fritts, D. C., and M. J. Alexander (2003), Gravity wave dynamics and effects in the middle atmosphere, *Rev. Geophys.*, *41*(1), 1003, doi:10.1029/2001RG000106.

Gille, J., J. Barnett, J. Whitney, M. Dials, D. Woodard, W. Rudolf, A. Lambert, and W. Mankin (2003), The High Resolution Dynamics Limb Sounder (HIRDLS) experiment on aura, *Proc. SPIE Int. Soc. Opt. Eng.*, *5152*, 162–171.

Gille, J., et al. (2008), High Resolution Dynamics Limb Sounder: Experiment overview, recovery, and validation of initial temperature data, *J. Geophys. Res.*, *113*, D16S43, doi:10.1029/2007JD008824.

High Resolution Dynamics Limb Sounder Team (2008), High Resolution Dynamics Limb Sounder Earth Observing System (EOS): Data description and quality version 3.00, report, NASA Jet Propul. Lab., Pasadena, Calif.

Hitchman, M. H., J. C. Gille, C. D. Rodgers, and G. Brasseur (1989), The separated polar winter stratopause: A gravity wave driven climatological feature, *J. Atmos. Sci.*, *46*, 410–422.

Hoffmann, P., W. Singer, D. Keuer, W. K. Hocking, M. Kunze, and Y. Murayama (2007), Latitudinal and longitudinal variability of mesospheric winds and temperatures during stratospheric warming events, *J. Atmos. Sol. Terr. Phys.*, *69*, 2355–2466.

Holton, J. R. (1983), The influence of gravity wave breaking on the general circulation of the middle atmosphere, *J. Atmos. Sci.*, *40*, 2497–2507.

Leutbacher, M., and H. Volkert (2000), The propagation of mountain waves into the stratosphere: Quantitative evaluation of three-dimensional simulations, *J. Atmos. Sci.*, *57*, 3090–3108.

Manney, G. L., et al. (2008a), The high arctic in extreme winters: Vortex, temperature, and MLS and ACE-FTS trace gas evolution, *Atmos. Chem. Phys.*, *8*(3), 505–522.

Manney, G. L., et al. (2008b), The evolution of the stratopause during the 2006 major warming: Satellite data and assimilated meteorological analyses, *J. Geophys. Res.*, *113*, D11115, doi:10.1029/2007JD009097.

Murgatroyd, R. J., and F. Singleton (1961), Possible meridional circulations in the stratosphere and mesosphere, *Q. J. R. Meteorol. Soc.*, *87*(372), 125–135.

Preusse, P., et al. (2006), Tropopause to mesopause gravity waves in August: Measurement and modeling, *J. Atmos. Sol. Terr. Phys.*, *68*, 1730–1751, doi:10.1016/j.jastp.2005.10.019.

Siskind, D. E., S. D. Eckermann, L. Coy, J. P. McCormack, and C. E. Randall (2007), On recent interannual variability of the Arctic winter mesosphere: Implications for tracer descent, *Geophys. Res. Lett.*, *34*, L09806, doi:10.1029/2007GL029293.

Smith, A. K. (1996), Longitudinal variations in mesospheric winds: Evidence for gravity wave filtering by planetary waves, *J. Atmos. Sci.*, *53*(8), 1156–1173.

Stockwell, R. G., L. Mansinha, and R. P. Lowe (1996), Localization of the complex spectrum: The S transform, *IEEE Trans. Signal Process.*, *44*(4), 998–1001.

J. J. Barnett, S. M. Osprey, and C. J. Wright, Atmospheric, Oceanic, and Planetary Physics, Department of Physics, University of Oxford, Parks Road, Oxford OX1 3PU, UK. (wright@atm.ox.ac.uk)

J. C. Gille, Center for Limb Atmospheric Sounding, University of Colorado at Boulder, Boulder, CO 80309-0440, USA.

L. J. Gray, Department of Meteorology, University of Reading, Earley Gate, PO Box 243, Reading RG6 6BB, UK.